Proc. Natl. Acad. Sci. USA
Vol. 83, pp. 1315–1319, March 1986
Biophysics

Structure–activity relationship in vinculin: An IR/attenuated total reflection spectroscopic and film balance study

(membrane anchoring/protein surfacing/protein monolayer/membrane penetration/conformational equilibrium)

URS PETER FRINGELI†, PETER LEUTERT‡, HERBERT THURNHOFER§, MARIANNA FRINGELI‡, AND MAX M. BURGER§

†Institute for Physical Chemistry, University of Vienna, Währingerstrasse 42, A-1090 Vienna, Austria; ‡Laboratory for Physical Chemistry, Swiss Federal Institute of Technology, CH-8092 Zurich, Switzerland; and §Biocenter, University of Basel, CH-4056 Basel, Switzerland

Communicated by A. Frey-Wyssling, October 8, 1985

ABSTRACT **Surfacing and membrane-penetrating ability of vinculin and bovine serum albumin have been studied on a macroscopic level by means of a Langmuir film balance and on a molecular level by means of infrared attenuated total reflection spectroscopy. It is suggested that the driving force of the nonspontaneous process of membrane penetration by native vinculin is the spontaneous formation of rigid vinculin monolayers in the membrane. Lateral adhesion of vinculin molecules results from the formation of intermolecular pleated-sheet structures. Vinculin surface activity was found to result from an α-helical segment oriented approximately perpendicular to plane of the membrane. There is a conformational equilibrium between this helix and random structure. High ionic strength (110 mM) favors helix formation that leads to the >100-fold enhancement of surfacing velocity relative to the velocity observed at a lower ionic strength (10 mM). Vinculin has a second helical segment oriented parallel to the plane of the membrane that is in a conformational equilibrium with the pleated-sheet structure.**

Vinculin is a structural protein with a molecular weight of 130,000 found in many different cell types. Since it accumulates in focal contacts where microfilaments are anchored to the plasma membrane, it has been proposed that vinculin may be involved in linking actin filaments to membranes (1–6) in a manner similar to that of α-actinin (7). Thus cell motility and shape may be influenced by the activity of this protein. Despite some disagreement (8), the present hypothesis, based on the increased amount of phosphotyrosine in proteins of transformed and malignant cells, states that vinculin also is phosphorylated on tyrosine by v-src or c-src kinases (9), resulting in a loss of focal contact and cell adhesion (4, 5).

Native vinculin shows a distinct tendency to surface with high velocity when injected into an aqueous subphase at physiological ionic strength, as do phospholipids, α-actinin (10), and other amphiphilic molecules. Surfacing velocity is drastically reduced at low ionic strength (10 mM Tris)—i.e., conditions under which it is solubilized from tissue homogenates (11). This is a reversible phenomenon, however, since vinculin was activated by increasing the ionic strength to physiological levels.

Here we report on ordered vinculin structures detected with a Langmuir film balance and with polarization IR spectroscopy and provide information on the molecular structures of native vinculin under physiological (active) and low (inactive) ionic strength as well as of acid-denaturated vinculin under physiological conditions.

The publication costs of this article were defrayed in part by page charge payment. This article must therefore be hereby marked "*advertisement*" in accordance with 18 U.S.C. §1734 solely to indicate this fact.

MATERIALS AND METHODS

Biochemicals. Vinculin was isolated from chicken gizzard (11). Denaturated vinculin was obtained by exposing the native form to 0.1 M HCl, pH 1.0, for 5 min. Bovine serum albumin (BSA) and bovine gamma-globulin were obtained from Fluka. Surface-bound (11S) acetylcholinesterase was isolated by the method of Hopff (12) and the membrane-incorporated form was isolated by the method of Stieger *et al.* (13). Palmitoylpalmitoleoylphosphatidylcholine and tripalmitin were from Berchtold (Bern, Switzerland).

Air-Water Interface Studies. A Langmuir film balance from MGW LAUDA (Lauda-Königshofen, Federal Republic of Germany) was used for kinetic studies of protein surfacing and protein penetration into a compressed lipid monolayer (membrane penetration). Information on the surfacing velocity was obtained by injecting 100 μl of protein solution (0.4 mg/ml in 10 mM Tris·HCl, pH 7.6) into the subphase (10 mM Tris·HCl or 10 mM Tris·HCl and 100 mM NaCl, pH 7.6) 5 mm beneath the clean air–water interface. The adjustable barrier (sweep) of the film balance was in the expanded position ($\approx$450 cm^2) to enable the protein molecules to enter the inferface without hinderance. A measure for the amount of surfaced protein was the area A of the monolayer at 20 mN/m. Therefore, at given time t the sweep was moved to compress the protein layer to this pressure. Immediately after this the sweep was moved again to the initial position. For protein penetration measurements, first the lipid was spread at the air–water interface and compressed to 15 mN/m, then the protein was injected into the subphase as described above. Since the film pressure was maintained constant by means of a servosystem, protein penetration enlarged the monolayer area $A(t)$. Rate constants of protein surfacing and monolayer penetration were determined from the A vs. t curves.

Protein Immobilization. The surface activity of BSA and of vinculin at physiological conditions enabled application of the Langmuir–Blodgett (LB) technique (14) to transfer monolayers from the air–water interface to the attenuated total reflection (ATR) plate at a constant pressure of 15 mN/m. Surface-inactive proteins, however, had to be immobilized by adsorption to a germanium ATR plate pretreated with aminopropyltriethoxisilane (15). While single monolayers could be transferred accurately by the LB technique, the adsorption technique has led to film thickness from 0.71 to 2.29 layers (*cf.* Table 1).

IR/ATR Spectroscopy. For detailed information on IR/ATR membrane spectroscopy see ref. 16. A homemade single-beam sample-reference grating spectrometer with a resolution of <2 cm^{-1} was used. Calculation of surface

Abbreviations: ATR, attenuated total reflection; BSA, bovine serum albumin; LB, Langmuir–Blodgett.

concentration of the immobilized protein was performed as described (17).

RESULTS

Surface Behavior

Surfacing Velocity. By determination of the half-life of the surfacing process, two classes of proteins were distinguished, a high surface-active class with a half-life <2 min and a low surface-active class surfacing at less than 1% of the rate of the high surface-active class (data not shown). Only vinculin at physiological conditions and BSA exhibited high surfacing velocity. However, in contrast to BSA, vinculin lost more than 99% of its original surfacing velocity when the ionic strength was reduced (10 mM Tris). Corresponding half-life was found to be 4.7 hr, a value also typical for acetylcholinesterase, bovine gamma-globulin, and acid-denaturated vinculin. Among the low-activity proteins, only native vinculin regained high activity when the ionic strength was increased from 10 to 110 mM. A detailed analysis is given in ref. 18.

Penetration of Compressed Lipid Monolayer. To investigate whether high surface activity necessarily includes the ability to penetrate lipid monolayers, native vinculin and BSA were injected into a subphase beneath a compressed monolayer (15 mN/m) of palmitoylpalmitoleoylphosphatidylcholine under physiological conditions. No significant change in the area of the lipid monolayer was observed with BSA. Vinculin, however, immediately led to an increase in the monolayer area of a monolayer maintained under constant pressure. Fifty percent of the surface-active vinculin was found to be membrane surface active—i.e., able to penetrate into the lipid layer. This part was composed of two equal populations—e.g., one having a high membrane surface activity and one having a low membrane surface activity. The corresponding half-lives of penetration were 1.6 min and 17 min. (For more details see ref. 18.)

Lateral Association of Vinculin. Another experimental approach indicates that the vinculin that enters the air–water interface forms a rigid layer of intermolecular aggregates. Injection of vinculin into the channel or a chamber between two surface compartments of a LB trough (10) led to a rigid vinculin surface layer. This surface layer is termed rigid because changes in surface pressure in one compartment were no longer transmitted to the neighboring compartment. A lipid monolayer did not have to be present before the injection of vinculin for the rigid vinculin surface layer to form, as was found earlier for α-actinin (10). Vinculin alone surfaces in the channel, forms the rigid layer, and if connected to both side compartments with phospholipids, does not incorporate these phospholipids. Even if injected beneath a phospholipid monolayer it surfaces, creating a pure vinculin layer in which no phospholipid can be detected by the Bligh and Dyer method (19). It should be noted that vinculin at low ionic strength (20 mM NaCl) and acid-denaturated vinculin were not able to form the rigid monolayer.

Structural Features

Vinculin samples were investigated in contact with liquid ^2H_2O, in the hydrated state [$N_2/^2H_2O$(g), relative humidity 90%, 25°C], and in a dry N_2 atmosphere by IR/ATR spectroscopy. No significant vinculin structural changes occurred when environments were exchanged, because the structural

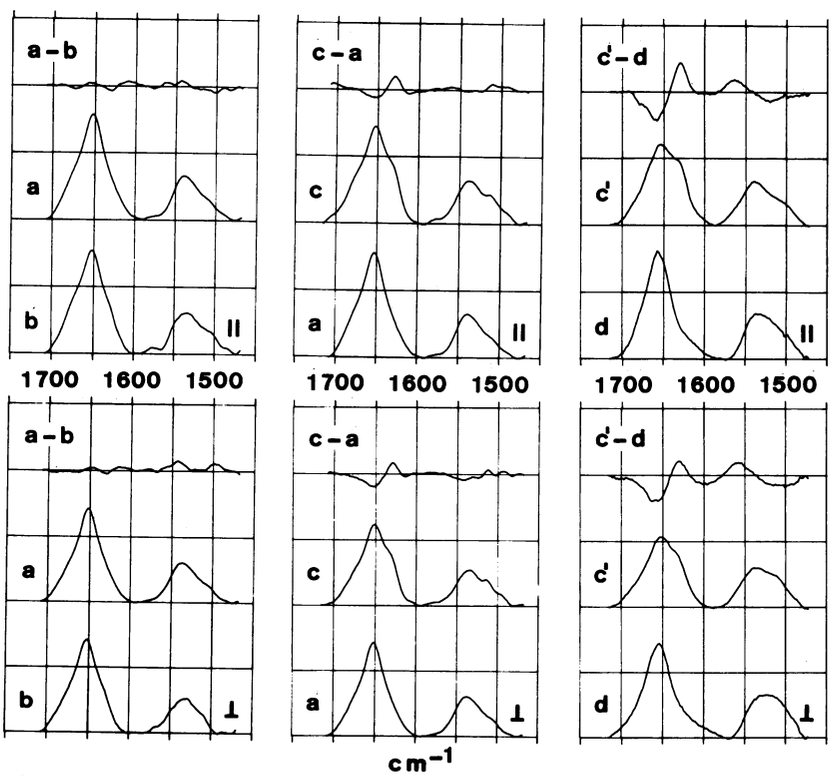

FIG. 1. IR/ATR spectra of immobilized vinculin and BSA in the amide I and II regions. Traces: a, native vinculin adsorbed at low ionic strength (10 mM, surface-inactive); b, acid-denatured vinculin, adsorbed at low ionic strength (10 mM NaCl, surface-inactive); c, native vinculin, LB monolayer (15 mN/m), transferred at high ionic strength (110 mM, surface-active); c', like trace c, however, independent sample; d, BSA, LB monolayer (15 mN/m), transferred at high ionic strength (110 mM, surface active). Difference spectra: a − b, c − a, and c' − d. Samples were prepared at pH 7.6. Spectra were obtained from dry samples [N_2(g)], T = 25°C. Ge-ATR plate, θ = 45°, parallel (||), and perpendicular ($\perp$) polarized incident light. Calibration was 0.08 absorbance units per digit, and the absorbance $A = -\ln T$. The intensity of the LB monolayer (trace c) was originally 1.59 nmol of amide groups/cm^2, the other spectra have been adjusted to this intensity (Table 1).

state at the moment of immobilization remained conserved. Thus the structural analysis presented in this paper is mainly based on spectra obtained from dry protonated samples.

Difference Spectra. Typical IR/ATR spectra in the amide I and II regions of native surface-inactive (trace a), native surface-active (traces c and c'), and denaturated surface-inactive (trace b) vinculin, as well as of surface-active (trace d) BSA, which was used as reference are shown in Fig. 1. The a − b difference spectra reflect structural changes in native vinculin that block surface activation by high ionic strength. From the band intensity, it is found that about 6% (i.e., 70) of the amino acids are involved. Native surface-inactive vinculin has excess absorbance near 1650 cm^{-1} [random and/or α-helix (20, 21)], whereas denatured surface-inactive vinculin has excess absorbance at 1632 cm^{-1} [β-pleated sheet (20, 21)] and at 1669 cm^{-1} [irregularly packed helix (22)]. The more prominent difference bands in the 1500–1600 cm^{-1} region have not been assigned so far.

Fig. 1, trace c shows the IR/ATR spectra of one LB monolayer transferred at a constant pressure of 15 mN/m. Comparison with native surface-inactive vinculin gives the first information on the structural elements responsible for surface activity. The c − a difference spectrum shows a considerable increase (≈10%, i.e., ≈117 amino acids) in β-structure (1632 cm^{-1}) in surface-active vinculin on charge of the 1650 cm^{-1} component which is more prominent in surface-inactive vinculin, and there is some evidence for a parallel polarized weak band near 1680 cm^{-1}. From these data, together with the unpolarized 1632 cm^{-1} band, one may conclude that there is an antiparallel pleated-sheet structure with a chain direction approximately perpendicular to the ATR plate.

The c' − d difference spectrum of the two surface-active proteins, BSA (Fig. 1, trace d) and native vinculin in 100 mM NaCl, 10 mM Tris (Fig. 1, traces c and c'), should reveal the structural requirements for membrane penetration. Obviously, there is a nearly complete lack of β-pleated sheet structure in BSA, which was found to be unable to penetrate a compressed lipid layer. On the other hand BSA has an excess of the 1659-cm^{-1} component, pointing most probably to helical structure. High helix content has been reported from CD measurements (23). Therefore, we suggest that the pleated-sheet structure of vinculin plays a significant role in its membrane incorporation, especially when the β-structure is of intermolecular origin, which leads to a rigid monolayer by lateral association.

Band Shape Analysis. The separation of overlapping bands into single components is a problem often encountered in quantitative analysis (see ref. 24). In this paper a band shape analysis of the amide I band (≈80% C=O stretching of the amide group) was performed. This band is centered between 1650 and 1660 cm^{-1}, the typical range for random and/or helical conformation. In most cases overlapping is too large for good separation of the contributions from random and helical structures by band shape analysis. β-Pleated sheet structures, however, can be separated without difficulty because of band shifts of 20–30 cm^{-1}. Uncertainties are often encountered in the amide I band wings due to overlaps with the absorption of other residues [≥1690 cm^{-1}, amides, carboxylic acids; ≤1620 cm^{-1}, amides, amines, aromatic residues (25)]. The analysis was guided by the following strategies: (*i*) To reduce the uncertainties in the band wings, the spectral range of amide I was reduced from ≈1695 to 1620 cm^{-1}. (*ii*) The number of components was equal to the number of peaks and wings visible in original spectra or difference spectra. In Fig. 2, trace a three components can easily be detected by visual inspection. A fourth component is expected at ≈1670 cm^{-1} from comparison of the parallel

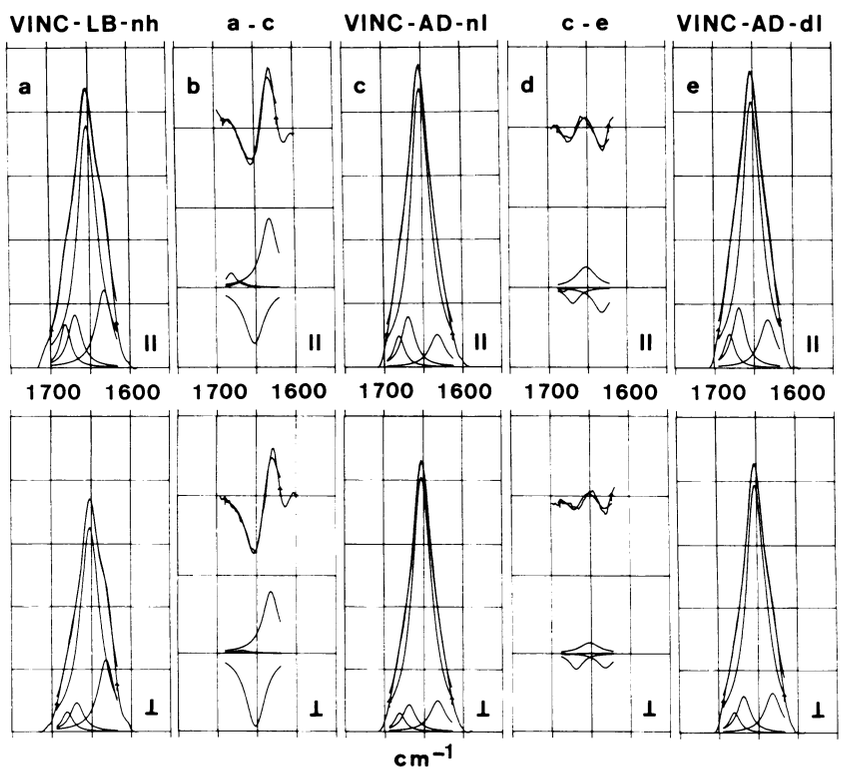

FIG. 2. Band shape analysis of the amide I band of native surface-active (trace a, sample 1), native surface-inactive (trace c, sample 4) and denatured surface-inactive (trace e, sample 5) vinculin, and of the difference spectra (a − c, sample 7) and (c − e, sample 6). Identical set of four Lorentzian bands (Table 1). Dry samples [N_2(g)], T = 25°C, Ge-ATR plate, θ = 45°, parallel (||) and perpendicular (⊥) polarized incident light. Calibration was 0.0267 absorbance units per digit for samples a, c, and d and 0.0222 absorbance units per digit for b and d (absorbance $A = -\ln T$). The intensities correspond to a vinculin LB monolayer at a constant pressure of 15 mN/m.

Table 1. Results and analysis of line-shape fitting of the amide I band

Sample no.	Vinculin treatment*	Layers† no.	Overall dichroic ratio	Band position/½ half-width (cm^{-1}) 1681/8 A, %	R	θ	1669/10 A, %	R	θ	1652/15‡ A, %	R	θ	1632/12 A, %	R	θ
1	LB layer on Ge-ATS, 110 mM, surface-active	1	1.22	9	2.13	0^{-0}_{+2}	12	1.78	19^{-2}_{+2}	65	1.16	53^{-2}_{+2}	15	1.05	69^{-9}_{+21}
2	Adsorbed to hydrophobic surface of 1 tripalmitin monolayer (ZnSe), 110 mM, surface-active	0.87	1.12† (1.23)	10	1.13† (1.24)	46^{-2}_{+2}	11	1.85† (1.88)	15^{-2}_{+2}	65	1.12† (1.23)	47^{-2}_{+2}	14	0.85† (0.99)	90^{-20}_{+20}
3	Adsorbed to Ge-ATS, 110 mM, surface-active	2.29	1.03	9	1.80	18^{-4}_{+3}	10	1.10	60^{-11}_{+29}	67	1.03	73^{-9}_{+17}	14	0.93	90^{-31}_{+0}
4	Adsorbed to Ge-ATS, 10 mM, surface-inactive	1.84	1.14	6	1.64	25^{-2}_{+3}	13	1.83	17^{-2}_{+2}	75	1.08	63^{-4}_{+4}	6	1.03	72^{-9}_{+18}
5	Adsorbed to Ge-ATS, acid-denaturated, 10 mM, surface-inactive	0.71	1.13	6	1.60	26^{-2}_{+3}	14	1.60	26^{-2}_{+3}	69	1.05	70^{-6}_{+4}	11	1.18	51^{-4}_{+3}
6	Difference spectra, sample 4 − 5	—	—	NS	NS	NS	−2	1.03	74^{-23}_{+16}	6	1.67	24^{-4}_{+3}	−5	1.82	18^{-7}_{+6}
7	Difference spectra, sample 1 − 4	—	—	≈2	NS	≈0	NS	NS	NS	−9	0.80	[90]§	9	1.02	76^{-23}_{+14}

The relative amount (A), the dichroic ratio (R), and the mean angle (θ, measured in degrees) between the transition moment and the normal to the plate were measured. Using the LB layer (sample 1) transferred at a constant pressure of 15 mN/m, the surface concentration of vinculin was $\Gamma = 1.33 \times 10^{-12}$ mols per cm^2 (17). The R was calculated from the absorption coefficients (16). The assumed order parameter (S) was equal to 0.6 (16). NS, not significant.

*LB, Langmuir–Blodgett (14); Ge-ATS, propyl-amino triethoxisilane-treated germanium-ATR plate; T, 25°C; ionic strength (mM).

†Dichroic ratio obtained with a ZnSe-ATR plate. Values in parenthesis correspond to the Ge-ATR plate.

‡Superimposed band cannot be separated by line-shape fitting.

§$\theta = 90°$ corresponds to $R = 0.99$. $R < 0.93$ is only possible for difference spectra, indicating that the subtrahend (sample 4) has an excess of horizontal transition moments (i.e., perpendicular-polarized ATR band, helix α_2).

and perpendicular polarized spectra. (*iii*) The frequencies and half-widths of the four components have to be the same for all vinculin samples, included in the difference and dichroic difference spectra. Best fit was achieved by using four Lorentzian bands. Parameters, results, and analysis of data are presented in Table 1, whereas Fig. 2 shows some typical examples of fitted bands.

Dichoric Analysis. The dichroic ratio (R) as defined by Eq. 1 contains the relevant information for orientation measurements (16). For an isotropic sample (order parameter $S = 0$) it follows that $R_{iso}^{ATR} = (E_x^2 + E_z^2)/E_y^2 = 1.14$ [Ge-ATR plate: $n_1 = 4$; protein layer: $n_2 = 1.5$; N_2(g): $n_3 = 1.0$; angle of incidence: $\theta = 45°$]. Deviation of R from R_{iso}^{ATR} reveals ordered structures, enabling calculation of the angle between the transition moment and the normal to the plate (Table 1). Obviously, the 1652-cm^{-1} component also contains ordered, most probably helical, structures. Moreover, the difference spectrum between samples 4 and 5 (Table 1) results in a parallel polarized band ($R = 1.67$), whereas the difference between samples 1 and 4 is a perpendicular polarized band ($R = 0.80$). Therefore, the 1652-cm^{-1} component is expected to result from three structural elements: random (denoted by ρ), one helix oriented approximately perpendicular (denoted by α_1), and a second helix oriented approximately parallel (denoted by α_2) to the ATR plate. This finding is confirmed by dichroic difference spectra D^*, i.e., the difference between the parallel polarized spectrum and the perpendicular polarized spectrum expanded by R_{iso}^{ATR}: $D^* = A_{\parallel} - R_{iso}^{ATR} \cdot A_{\perp}$. Thus D^* spectra are free of isotropic components. In acid-denaturated vinculin the overall 1652-cm^{-1} component is reduced to one negative band, pointing to transition moments oriented parallel to the ATR plate, i.e., the horizontal helices α_2. The amount was 26 ± 3% as concluded from the band area. Since the overall component amounts to 69 ± 2% (Table 1), the random (ρ) content is 43 ± 3%. D^* spectra of native vinculin exhibit two remaining bands of the 1652-cm^{-1} overall component, a negative one at 1652 cm^{-1} (α_2) and a positive one at 1656 cm^{-1} (vertical helix α_1). Overlapping of α_1 and α_2 was too great for separation by bandshape analysis; however, significant determination of the amounts was possible by means of Eq. 1 that enables calculation of the dichroic ratio of a band consisting of N overlapping components with fractions x_i, relative transition moments $m_i = M_i/M_1$ (M_i, effective transition moment of ith component), order parameters S_i, and angle θ_i between transition moment M_i and the normal to the ATR plate (z axis). E_x, E_y, and E_z are the electric field components. Deviation of Eq. 1 is based on the assumption of a liquid crystalline ultrastructure with the z axis as preferred orientation (16). First application of Eq. 1 was made in ref. 26.

$$R_z^{ATR} = \frac{A_{\parallel}}{A_{\perp}} = \frac{\sum_{i=1}^{N} x_i m_i^2 \left(E_x^2 \left[S_i \left(\frac{1}{2} \sin^2 \theta_i - \frac{1}{3} \right) + \frac{1}{3} \right] + E_z^2 \left[S_i \left(\cos^2 \theta_i - \frac{1}{3} \right) + \frac{1}{3} \right] \right)}{\sum_{i=1}^{N} x_i m_i^2 E_y^2 \left[S_i \left(\frac{1}{2} \sin^2 \theta_i - \frac{1}{3} \right) + \frac{1}{3} \right]}.$$

Further analysis is straightforward. It follows from Table 1 that the β-structure (denoted by β) is in equilibrium with the 1652-cm^{-1} overall component; i.e., $\beta \rightleftarrows \alpha_1$, $\beta \rightleftarrows \alpha_2$, or $\beta \rightleftarrows \rho$, paralleled by internal conversions $\alpha_1 \rightleftarrows \alpha_2$, $\alpha_1 \rightleftarrows \rho$, or $\alpha_2 \rightleftarrows \rho$. To find conversions that are consistent with the data in Table 1, one has to start with the separated components of

acid-denaturated vinculin (α_1, 0%; α_2, 26%; ρ, 43%). Proceeding to native vinculin (sample 4, Table 1) 5% converted β-structure has to be added to α_1, α_2, or ρ in such a way that the overall dichroic ratio calculated by Eq. **1** equals the value of the 1652-cm^{-1} component of Table 1. From sample 4 one proceeds to sample 1, etc. The following model turned out to be consistent with all original and difference spectra: $\beta \rightleftarrows \alpha_2$, $\alpha_1 \rightleftarrows \rho$, helix α_1 is inclined by about 20° from the normal to the ATR plate. The corresponding amounts were found to be as follows: for native surface-inactive vinculin [(sample 4, Table 1) α_1, 6 ± 3%; α_2, 31 ± 2%; ρ, 38 ± 3%], for native surface-active vinculin on a hydrophilic surface [(sample 1, Table 1) α_1, 15 ± 3%; α_2, 21 ± 2%; ρ, 29 ± 3%], and for same sample on a hydrophobic surface [(sample 2, Table 1) α_1, 22 ± 3%; α_2, 21 ± 2%; ρ, 22 ± 3%].

DISCUSSION

Three forms of vinculin have been investigated: a native surface-active vinculin that was able to penetrate compressed lipid layers, a native surface-inactive vinculin that could be activated by increasing the ionic strength, and an acid-denaturated vinculin that showed no response to ionic strength changes. BSA was used as surface-active reference protein that was not able to penetrate a compressed lipid layer. The main difference between surface-active vinculin and BSA was the lack of antiparallel pleated-sheet structure of the latter. We suggest that the β-structure of vinculin is formed as a result of intermolecular interaction upon lateral association. Assuming that (*i*) vinculin (V) can penetrate into the membrane (m) from the adsorbed state (a), $V_a \rightleftarrows V_m$ (equilibrium constant, K_o), and (*ii*) lateral assembly, $2\,V_m \rightleftarrows V_{m_2}, \ldots, V_{m_{n-1}} + V_m \rightleftarrows V_{m_n}$ (n, degree of assembly; K_i, equilibrium constant of the ith step), one can expect a spontaneous process of lateral assembly ($\Delta G_n < 0$) and a nonspontaneous step for monomer incorporation ($\Delta G_o > 0$). The former, however, should result in a spontaneous overall reaction ($\Delta G_o + \Delta G_n < 0$). Surface activity is found to be related to helix α_1 that is found to be in equilibrium with random structure ρ. Enhancement of ionic strength and hydrophobic environment led to helix α_1 formation. Short acid treatment, however, induced complete α_1 unfolding. Reactivation by high ionic strength was no longer possible, most probably due to refolding problems. This interpretation is supported by the fact that acid-denaturated vinculin becomes at least partly native again after several weeks of storage at 4°C. Finally, it should be mentioned that α_1 has the same direction as the irregular helix absorbing at 1669 cm^{-1}. Possibly this part could be the top of the regular α_1 helix at 1656 cm^{-1}.

We thank P. Burn for the vinculin isolation. Stimulating discussions with Dr. R. K. Meyer and Prof. Hs. H. Günthard are kindly acknowledged. U.P.F. thanks the directorate of the Laboratory for Physical Chemistry, Eidgenössische Technische Hochschule, for facilitating experimental work in their institute. Financial support by the Krebsliga des Kantons Zürich, the Swiss National Foundation, and the Roche Research Foundation is kindly acknowledged.

1. Geiger, B., Tokuyasu, K. T., Dutton, A. H. & Singer, S. J. (1980) *Proc. Natl. Acad. Sci. USA* **77**, 4127–4131.
2. Geiger, B., Dutton, A. H., Tokuyasu, K. T. & Singer, S. J. (1981) *J. Cell. Biol.* **91**, 614–628.
3. Burridge, K. & Feramisco, J. R. (1980) *Cell* **19**, 587–595.
4. David-Pfeuty, T. & Singer, S. J. (1980) *Proc. Natl. Acad. Sci. USA* **77**, 6687–6691.
5. Shriver, R. & Rohrschneider, L. (1981) *J. Cell. Biol.* **89**, 525–535.
6. Jockusch, B. M. & Isenberg, G. (1981) *Proc. Natl. Acad. Sci. USA* **78**, 3005–3009.
7. Burn, P., Rotman, A., Meyer, R. M. & Burger, M. M. (1985) *Nature (London)* **314**, 469–472.
8. Antler, A. M., Greenberg, M. E., Edelman, G. M. & Hanafusa, H. (1985) *Mol. Cell. Biol.* **5**, 263–267.
9. Sefton, B. M., Hunter, T., Ball, E. H. & Singer, S. J. (1981) *Cell* **24**, 165–174.
10. Meyer, R. M., Schindler, H. & Burger, M. M. (1982) *Proc. Natl. Acad. Sci. USA* **79**, 4280–4284.
11. Feramisco, J. R. & Burridge, K. (1980) *J. Biol. Chem.* **255**, 1194–1199.
12. Hopff, W. H. (1976) *Vierteljahresschr. Naturforsch. Ges. Zurich* **121**, 233–260.
13. Stieger S., Brodbeck, U., Reber, B. & Brunner, J. (1984) *FEBS Lett.* **168**, 231–234.
14. Blodgett, K. B. & Langmuir, I. (1937) *Phys. Rev.* **51**, 964–982.
15. Hofer, P. & Fringeli, U. P. (1979) *Biophys. Struct. Mech.* **6**, 67–80.
16. Fringeli, U. P. & Günthard, Hs. H. (1980) in *Molecular Biology, Biochemistry and Biophysics*, Membrane Spectroscopy, ed. Grell, E. (Springer, Berlin), Vol. XXXI, pp. 270–332.
17. Fringeli, U. P. (1980) *J. Membr. Biol.* **54**, 203–212.
18. Leutert, P., Fringeli, U. P., Thurnhofer, H., Fringeli, M. & Burger, M. M. (1985) *J. Membr. Biol.*, in press.
19. Bligh, E. G. & Dyer, W. I. (1959) *Can. J. Biochem. Physiol.* **37**, 911–917.
20. Miyazawa, T. (1960) *J. Chem. Phys.* **32**, 1647–1652.
21. Parker, F. S. (1983) *Application of Infrared, Raman and Resonance Raman Spectroscopy in Biochemistry* (Plenum, New York).
22. Fringeli, U. P. & Fringeli, M. (1979) *Proc. Natl. Acad. Sci. USA* **76**, 3852–3856.
23. Reed, R. G., Feldhoff, R. C., Clute, O. L. & Peters, Th. (1975) *Biochemistry* **14**, 4578–4583.
24. Maddams, W. F. (1980) *Appl. Spectrosc.* **34**, 245–267.
25. Simons, L., Bergström, G., Blomfelt, G., Forss, S., Stenbäck, H. & Wansén, G. (1972) *Commentat. Phys. Math. Soc. Sci. Fenn.* **42**, 125–207.
26. Gremlich, H. U., Fringeli, U. P. & Schwyzer R. (1983) *Biochemistry* **22**, 4257–4263.